frontiers in Neuroanatomy

METHODS
published: 20 November 2020
doi: 10.3389/fnana.2020.599282

Comparison of Transparency and Shrinkage During Clearing of Insect Brains Using Media With Tunable Refractive Index

Bo M. B. Bekkouche, Helena K. M. Fritz, Elisa Rigosi and David C. O'Carroll*

Department of Biology, Lund University, Lund, Sweden

Improvement of imaging quality has the potential to visualize previously unseen building blocks of the brain and is therefore one of the great challenges in neuroscience. Rapid development of new tissue clearing techniques in recent years have attempted to solve imaging compromises in thick brain samples, particularly for high resolution optical microscopy, where the clearing medium needs to match the high refractive index of the objective immersion medium. These problems are exacerbated in insect tissue, where numerous (initially air-filled) tracheal tubes branching throughout the brain increase the scattering of light. To date, surprisingly few studies have systematically quantified the benefits of such clearing methods using objective transparency and tissue shrinkage measurements. In this study we compare a traditional and widely used insect clearing medium, methyl salicylate combined with permanent mounting in Permount ("MS/P") with several more recently applied clearing media that offer tunable refractive index (n): 2,2′-thiodiethanol (TDE), "SeeDB2" (in variants SeeDB2S and SeeDB2G matched to oil and glycerol immersion, $n = 1.52$ and 1.47, respectively) and Rapiclear (also with $n = 1.52$ and 1.47). We measured transparency and tissue shrinkage by comparing freshly dissected brains with cleared brains from dipteran flies, with or without addition of vacuum or ethanol pre-treatments (dehydration and rehydration) to evacuate air from the tracheal system. The results show that ethanol pre-treatment is very effective for improving transparency, regardless of the subsequent clearing medium, while vacuum treatment offers little measurable benefit. Ethanol pre-treated SeeDB2G and Rapiclear brains show much less shrinkage than using the traditional MS/P method. Furthermore, at lower refractive index, closer to that of glycerol immersion, these recently developed media offer outstanding transparency compared to TDE and MS/P. Rapiclear protocols were less laborious compared to SeeDB2, but both offer sufficient transparency and refractive index tunability to permit super-resolution imaging of local volumes in whole mount brains from large insects, and even light-sheet microscopy. Although long-term permanency of Rapiclear stored samples remains to be established, our samples still showed good preservation of fluorescence after storage for more than a year at room temperature.

Keywords: transparency, shrinkage, insect brain, brain imaging, super-resolution microscopy, digital light-sheet, neuron imaging, optical tissue clearing

OPEN ACCESS

Edited by:
Marcello Rosa,
Monash University, Australia

Reviewed by:
Tingting Yu,
Huazhong University of Science and Technology, China
Karin Nordström,
Flinders University, Australia
Irene Costantini,
European Laboratory for Non-linear Spectroscopy (LENS), Italy

****Correspondence:***
Bo M. B. Bekkouche
bo.bekkouche@biol.lu.se

Received: *26 August 2020*
Accepted: *26 October 2020*
Published: *20 November 2020*

Citation:
Bekkouche BMB, Fritz HKM, Rigosi E and O'Carroll DC (2020) Comparison of Transparency and Shrinkage During Clearing of Insect Brains Using Media With Tunable Refractive Index. Front. Neuroanat. 14:599282. doi: 10.3389/fnana.2020.599282

INTRODUCTION

A number of technological advances in recent years have increased the desirability of imaging structures within the brain in high resolution using optical rather than traditional histological sectioning. Applications range from imaging neurons revealed via optogenetic techniques, to *in-situ* neuronal tracing in order to establish circuit level interactions between neurons (Dunbier et al., 2012; Keles and Frye, 2017). As an example, our lab has been applying biophysically realistic computational models for dendritic integration by neurons (Shoemaker, 2011; Bekkouche et al., 2017). Such models rely on high resolution 3D reconstruction of individual neuron morphologies within the brain, to establish the biophysical compartments through which neuronal signals travel. A general hypothesis in this type of modeling is that fine neurites perform important computations as part of the neural network. The higher the imaging quality, the greater the certainty that the morphology of all fine neurites and likely synaptic zones that contribute to the response are faithfully captured by the imaging system and can thus be incorporated into the model.

One challenge for the application of such *in-situ* optical imaging techniques, however, is the limitation to resolution caused by light scattering within the thick tissue sample. This requires the application of a suitable clearing medium (Silvestri et al., 2016; Ariel, 2017) to reduce local refractive index differences that provide the basis for such scattering (Schmitt and Kumar, 1998; Tuchin et al., 1998; Tuchin, 2005; Harvard et al., 2015). These problems are exacerbated in insect tissue by their tracheal respiratory system: numerous air-filled tracheal tubes branch finely throughout the brain increasing these index differences and thus scattering of light.

In insect neurobiology, several traditional clearing media such as terpineol and methyl salicylate have been widely applied for imaging thick Golgi stained or fluorescently labeled samples (Coss et al., 1980; Carrow et al., 1984; Kurylas et al., 2008; el Jundi et al., 2010; Lin and Strausfeld, 2012; Stöckl and Heinze, 2015; Adden et al., 2020). The dehydration of the brain with organic solvents required before clearing in such media generally aids displacement of air trapped in the tracheal system, leading to good tissue clarity. In many labs, it has become standard practice to permanently mount such methyl salicylate cleared samples using a hardening mounting medium such as Permount^{TM}, before imaging. This permits the very stable imaging required to combine multiple large volume image sets for whole brain reconstructions or for tracing neurons with processes that may travel up to several millimeters across the brain (Geurten et al., 2007; Kurylas et al., 2008; el Jundi et al., 2010). Another advantage of this method is that samples then survive storage for many years, and can subsequently be re-imaged using newly available techniques or even re-treated with new immunohistochemical analyses after dissolving out the mounting medium in a suitable solvent (Heinze and Homberg, 2008; Heinze et al., 2013).

While clearing in methyl salicylate/ Permount remains widely used, this technique is not without problems for insect brain imaging (Gonzalez-Bellido and Wardill, 2012). In particular, the high refractive index of the medium (1.52) requires the use of oil immersion objectives in order to avoid spherical aberration within the sample. While this permits high image resolution, this typically comes with a compromise of short working distance, often below 100 μm. This limits the useful depth that can be imaged at all and often requires samples to be flipped and re-imaged from both sides, complicating subsequent analysis. Oil immersion objectives are entirely unsuitable for whole-mount imaging of large organs such as rodent brains. Even in insects such as those studied in our own lab, the brains of larger species such as dipteran flies, bees and dragonflies are ∼500 μm thick even in their smallest dimension.

There are several partial solutions to improve the tradeoff between the high numerical aperture required for high resolution imaging and the large working distance required for imaging brains in whole mount. High numerical aperture objectives designed to work with cover-slipped samples offering several times the working distance of oil immersion have recently been produced by several vendors, using lower refractive index immersion media such as silicone oil or glycerol.

Successful application of such objectives to thick samples requires a clearing medium that not only provides good tissue clarity, but also with a refractive index to match the immersion medium and thus avoid spherical aberration that increases with imaging depth (Dong et al., 2004; Gonzalez-Bellido and Wardill, 2012). Several water-miscible clearing media have recently been introduced to provide a means to adjust refractive index and find the best combination of tissue clarity and objective immersion medium. One such medium, 2,2'-thiodiethanol (TDE) can be diluted with small volumes of water to match either glycerol or oil immersion (Staudt et al., 2007) and has been successfully applied to insect central nervous system tissue (Gonzalez-Bellido and Wardill, 2012).

While TDE may provide a suitable solution in some applications and can provide an excellent optical point-spread function deep within an embedded sample, it is known to quench the fluorescence of fluorophores such as eGFP at the large concentration required for high numerical aperture microscopy (Staudt et al., 2007; Ke et al., 2016). Ke et al. (2016) recently introduced a novel alternative, non-quenching clearing medium, "SeeDB2," based on iohexol, in variants that can either match immersion oil or glycerol. They demonstrated an excellent 3-dimensional point spread function, rivaling that of high concentrations of TDE and then successfully applied this to several super-resolution imaging applications, including on insect brain samples. Another new water soluble clearing medium recently introduced to insect brain research (Frank et al., 2017), Rapiclear (developed by Sunjin lab Co.), also has the advantage of tunable refractive index.

The water solubility of tunable media such as Rapiclear and SeeDB2 does not require a final dehydration stage before mounting and imaging. This potentially gives better control over tissue shrinkage. Tissue shrinkage is, of course, highly undesirable for super-resolution imaging or if the goal is to obtain accurate estimates of neurite diameters, as required for accurate compartment modeling of neurons.

To date there has been no systematic analysis of the pros and cons and cross-comparison of these recently developed methods

with traditional techniques. Few prior comparison studies have applied a mathematically based transparency measurement method (Wan et al., 2018; Yu et al., 2018; Loren et al., 2019; Xu et al., 2019). Loren et al. (2019) focused on comparing attenuation of transparency over time using an objective measurement of the transparency of different clearing media. Yu et al. (2018) discussed several new clearing media, but the transparency was not quantified between clearing techniques. Wan et al. (2018) compared seven clearing methods using a mathematical approach to calculate imaging depth based on intensity which could be considered as a measurement of transparency. Xu et al. (2019) quantified and compared both transparency and shrinkage in seven clearing media. However, none of these studies focused specifically on insect tissue, with the additional challenges presented by the tracheal respiratory system.

In this paper we developed a standard experiment protocol to quantify the trade-off between tissue transparency, refractive index and shrinkage or expansion artifacts using several of these recently developed clearing methods. We benchmarked these against the traditional methyl salicylate/Permount method. We measured transparency of brain images against a background grating to estimate the contrast attenuation by the tissue, then estimated shrinkage by identifying common reference points in images of large fly brains (from hoverflies and blowflies) before and after clearing. We found that among the newer clearing methods, both SeeDB2 and Rapiclear not only reduce shrinkage compared with methyl salicylate cleared brains, they also provide a substantially more transparent brain. In addition, the compatibility of Rapiclear with a range of direct-immersion objectives makes this an outstanding choice for new applications such as light-sheet microscopy.

MATERIALS AND EQUIPMENT

Table 1 provides a list of reagents/ materials and/or equipment specifically required for the methods we developed.

Methods

We developed clearing protocols to allow quantitative comparison of 2 variants of the iohexol based clearing medium SeeDB2 ("SeeDB2G," refractive index $n = 1.46$, "SeeDB2S" $n = 1.52$); several variants of Rapiclear (hereafter referred to as "Rapiclear*X.X*" where *X.X* is either $n = 1.47$, 1.49, or 1.52); 97% 2,2'-thiodiethanol ("TDE," $n = 1.52$); and methyl salicylate in combination with permanent mounting in Permount (n=1.52). Where appropriate, we also tested the effect of pre-treatment to reduce air trapped in tracheal tubes, either by vacuum treatment or by dehydration through an ethanol series followed by rehydration. Mann-Whitney-Wilcoxon non parametric test for two unpaired groups was used to generate p-values.

Species Used and Dissection Procedure

Animal species used were the large hoverflies *Volucella pelluscens, Eristalis tenax,* or the very similar *Eristalis pertinax,* and the blowfly *Calliphora vicina*. Although there is substantial variation between individuals, these all have similarly large

TABLE 1 | Reagents, materials and equipment required for the methods.

Material/equipment	Supplier/manufacturer
Phosphate buffered saline (PBS)	Amresco Inc. Solon, Ohio, USA
Methyl salicylate (MSC)	Sigma-aldrich, ST. Louis, USA
2,2′-thiodiethanol (TDE)	Sigma-aldrich, ST. Louis, USA
Rapiclear	Sunjin labs, Hsinchu City, Taiwan
Ethanol	CCS healthcare AB, Borlänge, Sweden
Cavity slides	Saveen werner AB, Limhamn, Sweden
Slides	Thermo scientific, Waltham, Massachusetts, USA
Cover slips	VWR international AB, Stockholm, Sweden
Calliphora	Blades Inc., Kent TN8 7DX, Cowden, Edenbridge, UK
Eristalis tenax	Polyfly SL, Avd. de la Innovación, 15 Ed.Pitágoras 3ª, 75, Parque Científico-Tecnológico de Almería (PITA), 04131 Almeria, SPAIN
Formaldehyde 4% in PBS, pH 7.4	Histolab Products AB, Gothenburg, Sweden
Histodenz	Sigma-aldrich, ST. Louis, USA
Tris-HCl	Merck, Darmstadt, Germany
Ethylenediaminetetraacetic acid (EDTA)	Sigma-aldrich, ST. Louis, USA
Triton x-100	Amresco Inc. Solon, Ohio, USA
Lucifer yellow CH	Sigma-aldrich, ST. Louis, USA
Alluminocilicate glass capilaries	Harvard apparatus, UK
Small glass vial	Glaswarenfabrik Karl Hecht Gmbh & Co KG, Sondheim, Germany
Plastic lid for small glass vial	Glaswarenfabrik Karl Hecht Gmbh & Co KG, Sondheim, Germany
Permount	Fisher scientific, New Jersey, USA
Double-sided sticker	Sunjin labs, Hsinchu City, Taiwan
Multiwell plate	SPL Lifesciences Co, Ltd, Pocheon-city, Korea
Biotin conjugated anti-lucifer antibody	Life technologies, Eugene, USA
Bovine serum albumin fraction V	Sigma-aldrich, ST. Louis, USA
Streptavidin Cy5	Life technologies, Eugene, USA
Streptavidin Cy3	Life technologies, Eugene, USA
Normal goat serum (NGS)	Life technologies, Eugene, USA
Dimethyl sulfoxide (DMSO)	Sigma-aldrich, ST. Louis, USA
Plastic spacers (Zweckform No. 3510)	Avery Zweckform, Germany
Self-adhesive spacers	Sunjin labs, Hsinchu City, Taiwan
Paraformaldehyde	Agar Scientific Ltd, Stansted, Essex, UK
Glutaraldehyde	Agar Scientific Ltd, Stansted, Essex, UK
Na-cacodylate buffer	TAAB laboratory equipment Ltd, Aldermaston, Berks, UK
Osmium tetroxide	Ted Pella Inc., Redding, California, USA
Ethanol	VWR Chemicals, Randor, Pennsylvania, USA
Agarose	MP Biomedicals Inc., Eschwege, Germany
Fluorescent nanobeads (diameter 200 nm)	Thermo Fisher Scientific, Waltham, MA USA
Nikon SMZ18 stereomicroscope	Nikon, Tokyo, Japan

(Continued)

TABLE 1 | Continued

Andor Zyla 5.5 USB 3.0 sCMOS camera	Andor, Belfast, UK
SHR Plan Apo 2x objective	Nikon, Tokyo, Japan
NBS 1952 Resolution Test Target, Background grating	Thorlabs, New Jersey, USA
Leica SP8 DLS confocal microscope	Leica Microsystems A/S, København, Denmark
HC PL APO CS2 20x/0.75 IMM immersion objective (oil)	Leica Microsystems A/S, København, Denmark
HC PL APO CS2 63x/1.3 glycerol objective	Leica Microsystems A/S, København, Denmark
HC PL FLUOTAR 5x/0.15 IMM objective	Leica Microsystems A/S, København, Denmark
DLS TwinFlect 7.8 mm	Leica Microsystems A/S, København, Denmark
HC PL APO CS2 63x/1.4 oil objective	Leica Microsystems A/S, København, Denmark
Sodium alginate (CAS Number 9005-38-3)	Sigma-aldrich, ST. Louis, USA

brains (freshly dissected dimensions ∼3,000 by 1,500 by 400μm), providing a suitable challenge for both objective lens working distance and the tissue clarity required for deep imaging. In total 71 flies were included in our analysis: 8 wild-caught *Volucella*, 23 wild *Eristalis spp.* (mostly *E. tenax*), 9 *E. tenax* hatched from pupae purchased from Polyfly and 31 *Calliphora* hatched from pupae purchased from Blades Inc. Another single *Eristalis* was used as an example application of intracellular dye injection for light sheet and high-resolution imaging. All animals/brains are labeled with an id (for example #01) which can be used to find meta-data in the **Supplementary Table** (see Excel **Supplementary File 1**).

Many of the animals utilized were part of ongoing acute experiments and electrophysiological analysis or intracellular labeling of neurons for other projects, hence the sample of flies used are typical of real experimental scenarios and conditions. Following experiments, the animal was decapitated and the brain was extracted by dissection under 0.1 M phosphate buffered saline, pH 7.4 (PBS) and transferred into a small glass vial with 4% formaldehyde in PBS for fixation overnight at 4°C.

Pre-treatment

Following fixation, brains were first imaged to identify morphological landmarks and a pre-treatment estimate of tissue clarity (see Transparency Measurement and Calculation below). All images were captured using a Nikon SMZ18 microscope with an SHR Plan Apo 2x objective (working distance 20 mm), with samples illuminated by diffuse incident light. Brains were then either pre-treated with ethanol (denoted by the subscript "$_E$" in figures and text below), vacuum ($_V$), both ($_{EV}$) or no pretreatment. Ethanol treatment consisted of dehydration and rehydration of the brain through an ethanol series diluted in PBS with steps of 50, 60, 70, 80, 90, 95, 100, 95, 90, 80, 70, 60, 50% ethanol each for 20 min on a shaker at room temperature. Note that the methyl salicylate /Permount clearing protocol (MS/P) always requires an ethanol dehydration series without subsequent rehydration since this medium is not miscible with water. In all other protocols, our application of the label $_E$ implies both dehydration and rehydration prior to clearing.

Vacuum treatment consisted of two 10 min treatments with the brain immersed in the PBS in a 5 ml glass vial with an open lid, placed in a vacuum chamber at a vacuum pressure of ∼75 kPa. The PBS was changed between treatments.

Clearing and Mounting

Following pre-treatment (if any), brains were then cleared according to the following protocols:

Rapiclear

After pre-treatment, brains were transferred into an eppendorf tube with 30–60 μL Rapiclear (Rapiclear1.52, 1.49, or 1.47) overnight on a shaker at room temperature. The brain was then mounted between two #1.5 coverslips (160μm thickness) using 500 μm self-adhesive spacers (Sunjin labs) with fresh Rapiclear applied from a transfer pipette to fill the well created by the spacer. The coverslips were then attached temporarily to a glass microscope slide using lab tape to permit imaging from either side, if desired.

Methyl Salicylate and Permount (MS/P)

Following dehydration through an ethanol series, brains were transferred from the plastic vial or well plate to a 5 ml glass vial, since methyl salicylate is a solvent for many plastics. A solution consisting of 50% ethanol and 50% methyl salicylate was added to the glass vial for 15 min. Finally, the brain was left on the shaker overnight at room temperature in 100% methyl salicylate. The following day brains were mounted between two coverslips using Permount. Plastic spacers (Avery Zweckform) were used rather than the self-adhesive spacers described above, since we found that the Permount reacted with the adhesive, generating additional bubbles in the mounted brain.

Iohexol: SeeDB2G and SeeDB2S

Following pretreatment, brains were cleared in a series of 33.3, 50, and 99.7% "Omnipaque" solution with 0.3% Triton x-100 diluted in Tris-EDTA buffer. For each step, the brain was left on the shaker at room temperature overnight (or at least 6 h for the first two steps). Omnipaque solution consisted of 56.2% iohexol (5-(N-2,3-Dihydroxypropylacetamido)-2,4,6-triiodo-N,N′-bis(2,3-dihydroxypropyl)isophthalamide, sold as "Histodenz") and 43.8% Tris-EDTA. Tris-EDTA consisted of 10 mM Tris-HCl (pH 7.6), 1 mM EDTA and distilled water. The SeeDB2S protocol is the same as SeeDB2G but with a final immersion in 70.4% iohexol solution instead of 56.2% (Ke et al., 2016). The brain was then mounted as for Rapiclear above, using fresh iohexol solution.

2,2′-thiodiethanol (TDE)

The brains were treated through a dilution series of TDE in PBS with increasing concentration of TDE by 10% every 30 min, to

a final concentration of 97% (Staudt et al., 2007). The brain was then mounted as for Rapiclear above, but using fresh TDE.

Transparency Measurement and Calculation

Images of each brain were captured before and after clearing using a Nikon SMZ18 stereomicroscope equipped with an Andor Zyla 5.5 sCMOS camera, using a 2x objective (working distance 20 mm). Images were captured from two focal planes. The first was adjusted to allow dimension measurements from the brain itself (**Figures 1A,B**). The second image was with the focal plane adjusted to the plane of a background grating placed below the sample as it was viewed through the imaged brain (**Figure 1C**). Using ImageJ, adjacent rectangular regions of interest (ROIs) were selected within light vs. dark parts of the images of the grating where it extended beyond the brain or where it was viewed through the imaged brain (**Figure 1C**). The average pixel intensity within these adjacent ROIs was used to estimate the average Michelson contrast in the image, *C*, where

$$C = \frac{I_{max} - I_{min}}{I_{max} + I_{min}} \quad (1)$$

I_{max} is the maximum intensity (light) and I_{min} is the minimum intensity (dark). The transparency (t) was calculated with the following equation:

$$t = \frac{C_{brain}}{C_{ctrl}} \quad (2)$$

where C_{brain} is the contrast of the grating within the brain and C_{ctrl} is the contrast outside the brain.

Hence t is a measure of the contrast attenuation through the total thickness of the sample. To account for the varying brain size (and thus thickness in the Z dimension) between individuals,

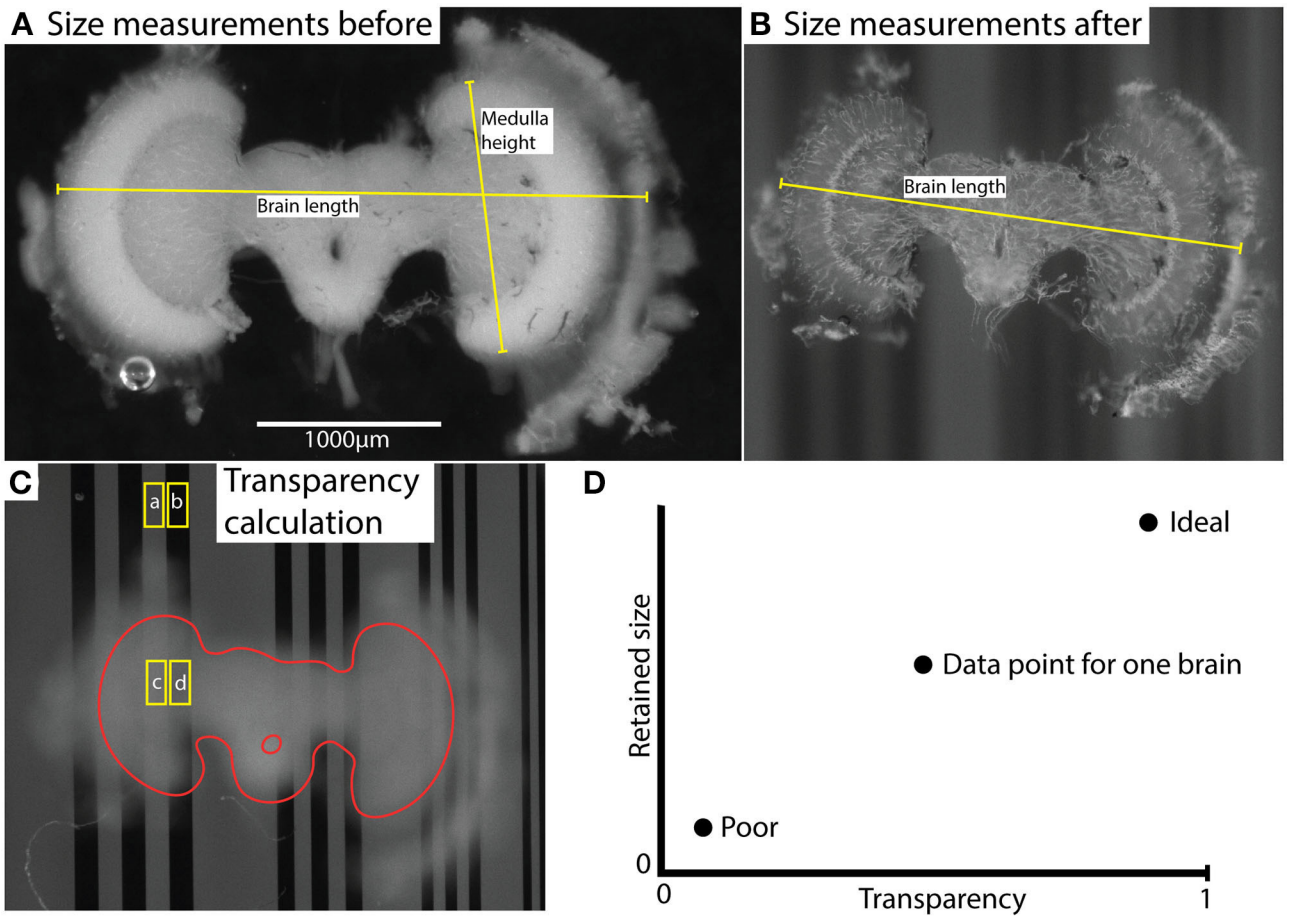

FIGURE 1 | Illustration of measurement method (using brain #45) and results. **(A,B)** illustrate size measurements for brain length and medulla height before **(A)** and after **(B)** clearing. "Brain length" indicates the typical length used for comparison of shrinkage. Characteristic landmarks rather than actual anatomical structure length were used to enable measurements on highly transparent brains. "Medulla height" indicates the length used for normalization of transparency values. This measurement was based on the anatomical height of the medulla and was measured only in uncleared brains. **(C)** shows selected areas (ROIs) used to calculate contrast; $C_{brain} = \frac{c-d}{c+d}$ and $C_{ctrl} = \frac{a-b}{a+b}$, and transparency $t = \frac{C_{brain}}{C_{ctrl}}$. The labels (a, b, c, d) indicate the average grayscale value of the area. The brain structure (excluding lamina) is outlined in red. **(D)** illustrates the interpretation of the comparative data plot (which is used in **Figure 4A**). Transparency and retained size are the two dimensions, and ideal vs. poor performance are indicated with two illustrative data points.

each transparency measurement (t) was normalized using the linear extent (h) of the medulla along the Y axis of the freshly fixed brain, a landmark that was consistently visible in every brain before clearing (as illustrated in **Figure 1A**). The following formula was then used:

$$t_{norm} = \mathrm{t}\frac{h}{h_{max}} \tag{3}$$

where h is the medulla height (see **Figure 1A** and Length Measurements for Shrinkage Estimation below) and h_{max} is the maximum medulla height measured among all brains analyzed.

Length Measurements for Shrinkage Estimation

The features used for size reduction estimation were selected so that the measurement coordinates corresponded to the same part of the brain as well as possible in every animal. Due to the very high transparency in certain brains after clearing, this was challenging at times. When possible, we measured the full width of the brain from edge to edge. **Figure 1A** shows an example of "Brain length" which was typically used. Typically, it was the distance between the extent of the lamina/outer medulla in the left and right hemispheres bound by landmarks at the edges of the brain. Suitable landmarks were first selected by visual examination of the cleared brain image and then identified in the corresponding image for the uncleared brain. In cases with extremely clear brains, we were sometimes forced to use the only landmarks clearly visible after clearing as reference points, such as small tears or other features at the margins of the dissected tissue or even individual tracheal tubes. Regardless of the landmarks used, we then computed the retained size (R):

$$R = \frac{D_{post}}{D_{pre}} \tag{4}$$

Where D_{post} is the length measurement obtained after pre-treatment and clearing, and D_{pre} is the length measurement obtained before treatment and clearing.

"Brain length" measurements were used for size reduction estimation, but as noted above, we used variable features in individual brains. We used a more standard feature of the brain size "Medulla height," as a normalizing parameter in transparency measurements to compensate for brain thickness. This "Medulla height" was only measured in the uncleared brains and was always calculated from a consistent feature visible in every brain, the distance between the upper and lower edges of medulla, as illustrated in **Figure 1A**. A straight line was manually adjusted on the images such that the length of the line was maximized, while remaining within the borders of the medulla.

These length or height measurements were not taken blinded and thus we acknowledge that this could introduce bias. This potential bias was however minimized by the fact that we were dealing with digitized images, enabling identification of the same landmarks to the nearest pixel before and after clearing.

Additional Experiments and Example Treatments

As part of our ongoing experiments, we intracellularly labeled several neurons (e.g., **Figures 5**, **6**) with a Lucifer yellow filled glass micropipette by injecting negative current (for details of the method, please see Barnett et al., 2007). The brains were then dissected, and fixed as above, then washed 4 × 10 min in PBS, 55 min in pure dimethyl sulfoxide, 3 × 30 min in PBS with 0.3% triton X-100 (PBT), 3 h with 5% natural goat serum (NGS) in PBT and then incubated for 3 days in biotin-conjugated anti-lucifer antibody diluted 50X in 2% NGS in PBT. The brains were then washed 3 × 30 min with 10% NGS in PBT, and then incubated for 3 days in streptavidin-Cy3 diluted 50X in 1% NGS in PBT. Finally, the brains were washed 3 × 30 min with PBS and cleared as described in section Rapiclear above (e.g., Rapiclear1.49$_{\mathrm{E}}$ for brain in **Figures 5**–**7**). Cleared brains were subsequently imaged using a Leica SP8 DLS confocal microscope and varying objectives and imaging modes. The microscopy images in **Figures 5A**, **7** were obtained using this microscope in its confocal mode. **Figures 5C**, **6** used the digital light sheet imaging mode (DLS), as illustrated in **Figure 5B**. Confocal objectives used were either a 20x/0.75 (magnification/numerical aperture) immersion objective (using oil) or a 63x/1.3 glycerol objective. **Figure 5C** (DLS mode) was imaged using a 5x/0.15 objective and DLS TwinFlect 7.8 mm mirrors both matched to the refractive index of glycerol (1.472).

Electron Microscopy Preparation Protocol

An additional 3 *Eristalis* brains were subjected to careful fixation as used in preparing samples for electron microscopy. Dissected brains were immersed in freshly prepared fixative solution, consisting of 2% paraformaldehyde and 2.5% glutaraldehyde in 0.1 M Na-cacodylate buffer (pH 7.4), for 24 h at 4°C. The brains were post-fixed in 1% osmium tetroxide in distilled water for 2 h at 4°C. The brains were dehydrated in graded ethanol series consisting of 70% ethanol (2 × 10 min), 96% ethanol (2 × 10 min), 100% ethanol (2 × 15 min). Brains were then transferred to acetone (2 × 20 min) as an intermedium before embedding first in dilute epoxy (Agar 100), with an acetone:epoxy mixture of (2:1) for 30 min, followed by 1:1 acetone:epoxy overnight, then infiltration with 100% epoxy for 8 h before polymerization for 48 h at 60°C. The final pictures were then photographed and brain lengths measured as for the cleared brains.

Point Spread Function in Rapiclear Using Nanobeads

To estimate the 3-dimensional point spread function at different depths within Rapiclear, we prepared samples incorporating fluorescent polystyrene nanobeads (diameter 200 nm). These were dispersed into 1% sodium alginate in distilled water at 45°C. Two microliter of this suspension was then applied to a well formed using a spacer as for whole mount imaging (see Rapiclear above). The alginate was then set to a permeable hydrogel to immobilize the beads by addition of 5 mM $CaCl_2$ in distilled water. Excess buffer was then pipetted off the sample before clearing directly in the well using Rapiclear1.47,

Rapiclear1.49, and Rapiclear1.52. Confocal images (Z series) were then captured using a Leica SP8 DLS with a 63x/1.3 glycerol objective (Rapiclear1.47 and 1.49) or a 63x/1.4 oil objective (Rapiclear1.52). Images were acquired using 2x oversampling in X, Y and Z with the photon counting mode of a hybrid detector, using a 0.5 Airy unit pinhole, 405 nm excitation and a narrow detection window between 470 and 510 nm. Five samples from each condition were captured and the axial and vertical full width at half maximum (FWHM) was calculated as follows. From each isolated bead image stack sample and condition the slice with the highest average intensity was selected for further processing. The FWHM was then measured by extracting a 1-dimensional intensity vector intersecting at the maximum intensity position, and then fitting this with a model for the PSF based on a Gaussian function convolved with 200 nm wide top-hat-function to allow for the near-resolvable size of the bead. For the curve fitting, the Matlab function "fit" (Matlab R2019b) with default settings (Non-linear least squares) was used. The following Gaussian was used:

$$g(x) = a + b * e^{-\frac{(x-\mu)^2}{2\sigma^2}} \quad (5)$$

where constant *a* is the luminance offset within the image, b is a scaling variable, μ is the x-axis center position, and σ is the standard deviation of the Gaussian.

The tophat-function was generated as a vector of zeros and ones using the Matlab function "rectpuls" (Matlab R2019b). The Gaussian was convolved with the Matlab function "conv" (Matlab R2019b), normalized and scaled with the following formulas:

$$y(x) = \text{conv}[\text{g (x)}, \text{rectpuls (x} - \text{e)}] \quad (6)$$

$$y = b * y/\max(y) \quad (7)$$

where constant e is the center position of the tophat-function and the conv-function used all constants for fitting. The FWHM was then extracted from the standard deviation variable in the Gaussian component of the fitted model using the following formula:

$$FWHM = 2\sqrt{2 * \ln(2)}\sigma \quad (8)$$

RESULTS

Qualitative Clearing Performance

Our protocol provides measurements of the effect of treatment (or pre-treatment) on changes in both brain dimensions (i.e., shrinkage or expansion) and transparency. Visual inspection of example brains cleared with Rapiclear1.52 and SeeDB2G but without ethanol treatment (**Figure 2**) clearly show that although more transparent than a fresh brain, the brains remain very visible as a cloudy foreground object, despite focusing on the background (**Figure 2** right column). Vacuum treatment to evacuate air from the tracheal system (Rapiclear1.52$_V$ and SeeEDB2G$_V$) provided no obvious improvement in transparency over untreated brains. However, pre-treatment by ethanol dehydration/rehydration (Rapiclear1.52$_E$ and SeeDB2G$_E$) dramatically improved transparency (**Figure 3**) to the extent that brains cleared using these media are barely visible at all when the background is in focus (**Figure 3** right column). Again, vacuum treatment made no apparent change to the transparency of ethanol pre-treated brains (Rapiclear1.52$_{EV}$ and SeeDB2G$_{EV}$) suggesting that ethanol dehydration is a more effective way to displace air from these tubes that contribute to scattered light. Although it is hard to measure, vacuum treatment could be decreasing the thickness of the larger tracheal tubes, which may not affect overall transparency much (as the results indicate), but may still improve imaging locally. Visual examination of a few samples of SeeDB2G, SeeDB2G$_V$, SeeDB2G$_E$, SeeDB2G$_{EV}$, Rapiclear1.52, Rapiclear1.52$_V$, Rapiclear1.52$_E$, and Rapiclear1.52$_{EV}$ indicates no difference in reduction in the thickness of the tracheal tubes (**Figures 2**, **3**, black patches and lines). Note that the vacuum chamber we had access to was not capable of providing a powerful vacuum, and the protocol provided by the manufacturer of Rapiclear recommended repeating 10 min of vacuum treatment 4 times for insect tissue, while we only performed 2 cycles. Hence it remains possible that additional vacuum treatment may further improve evacuation of the tracheal system.

Finally, we note that there is no apparent difference in transparency between Rapiclear and SeeDB2G cleared brains following ethanol pre-treatment, with both achieving very high transparency (**Figure 3** right column). The qualitative results we obtained for Rapiclear with ethanol pretreatment are impressive considering the simplicity and speed of the clearing protocol (direct transfer from buffer to the clearing medium).

Quantitative Clearing Performance

Figure 4A shows results obtained after applying the clearing method to each brain and quantifying both the transparency using a metric that takes individual variations in brain size (and thus depth) into account, plotted against the retained size (as a relative fraction of the original size, 1.0) to account for shrinkage. In this representation, an ideal clearing medium would produce both perfect transparency and minimal shrinkage, leading to points lying in the upper right of the graph (see **Figure 1D**). Clearing protocols with vacuum treatment showed no significant improvement over those without vacuum treatment ($p = 0.1738$ for Rapiclear1.52$_E$ [$n = 7$] vs. Rapiclear1.52$_{EV}$ [$n = 9$]) and were therefore pooled together into a single group. The traditional protocols MS/P, TDE, and the newer methods (Rapiclear1.47 and Rapiclear1.52) without ethanol treatment tended gave lower median transparency than Rapiclear1.47$_E$, Rapiclear1.52$_E$, SeeDB2G$_E$, and SeeDB2S$_E$ (summarized as Box and whisker plots, **Figure 4B**). Some clearing protocols, including MS/P and Rapiclear1.52$_E$ showed substantial variability in transparency between individuals (**Figure 4A**).

Although it gave little tissue shrinkage, TDE gave very low transparency compared to the clearing protocols, which surprised us due to the reported usefulness of this clearing medium (Gonzalez-Bellido and Wardill, 2012). In terms of the point-spread function (PSF) of nanobeads suspended in the medium, this was the best of the clearing media tested by Ke et al. (2016), although they did not report on absolute tissue clarity. Considering the reports that this medium also

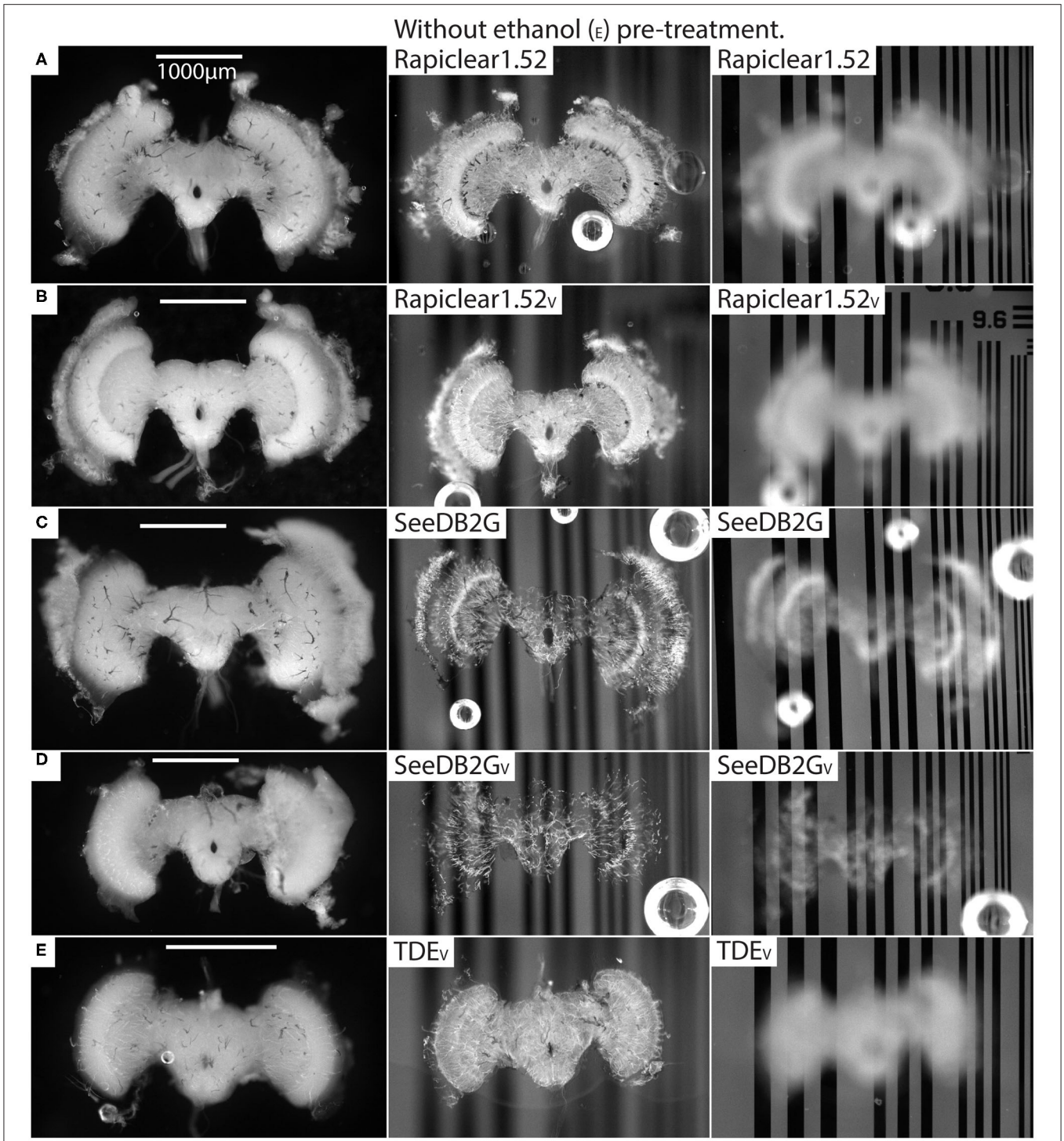

FIGURE 2 | Pre and post clearing pictures of brains cleared with and without vacuum treatment ($_V$). The uncleared brains are clearly visible in the left column and the cleared brains in the middle (brain in focus) and right (grating in focus) column are also visible. **(A)** is brain #56 (*Eristalis*), **(B)** is #46 (*Eristalis*), **(C)** is #67 (*Eristalis*), **(D)** is #69 (*Eristalis*), and **(E)** is #97 (*Calliphora*). Note that the brain size varies between samples **(A–E)** depending on species.

quenches fluorophores more than other protocols, it is difficult for us to recommend it for insect tissue, although perhaps tuning of the TDE concentrations or inclusion of ethanol pre-treatment could improve the transparency. That said, further addition of protocol stages would also make this protocol relatively complex compared with Rapiclear or SeeDB2

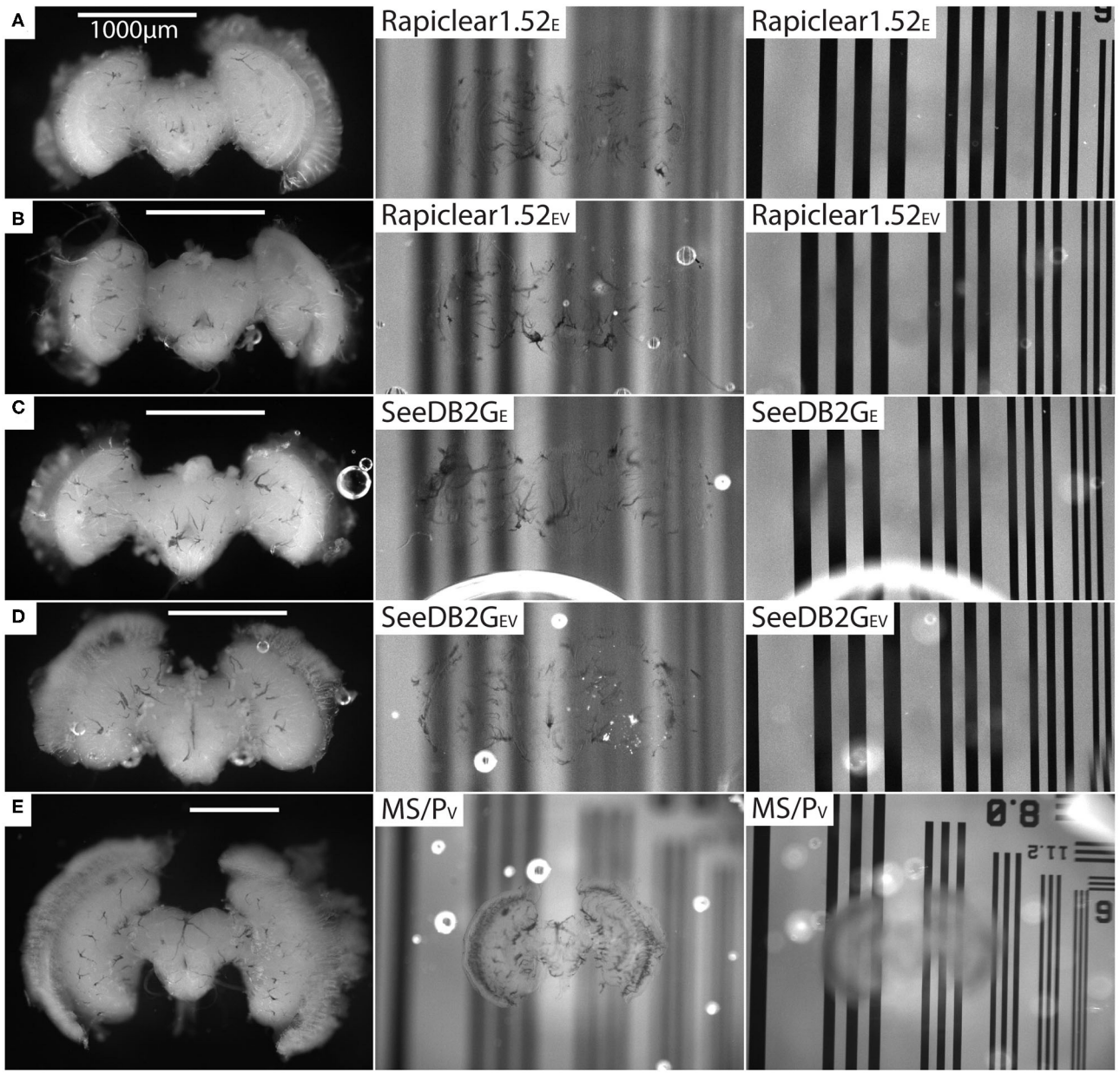

FIGURE 3 | Pre and post clearing pictures of brains cleared with and without vacuum treatment (V) (all with ethanol treatment [E]). Methyl salicylate with Permount is abbreviated as MS/P. The uncleared brains are clearly visible in the left column and the cleared brains are barely visible (tracheal tubes visible) in the middle (brain in focus) and right (grating in focus) column. **(A)** is brain #80 (*Calliphora*), **(B)** is #75 (*Calliphora*), **(C)** is #82 (*Calliphora*), **(D)** is #81, and **(E)** is #61 (*Eristalis*). Note that the brain size varies between samples **(A–E)** depending on species.

clearing, since it already involves progression through a slow TDE series. This could perhaps be amended if either the TDE and/or ethanol series were reduced by adding larger concentration increments at each step and reducing the waiting time between the steps, but given the superiority of the other techniques, we did not attempt further fine tuning of this protocol.

Refractive Index Dependent Transparency and Shrinkage Comparison

Clearing of tissue using the 4 agents we tested here works mainly by matching the refractive index of the medium to that of the tissue in order to reduce scattering. Water soluble media such as SeeDB2 and Rapiclear permit refractive index tuning by varying the concentration of the non-aqueous components of

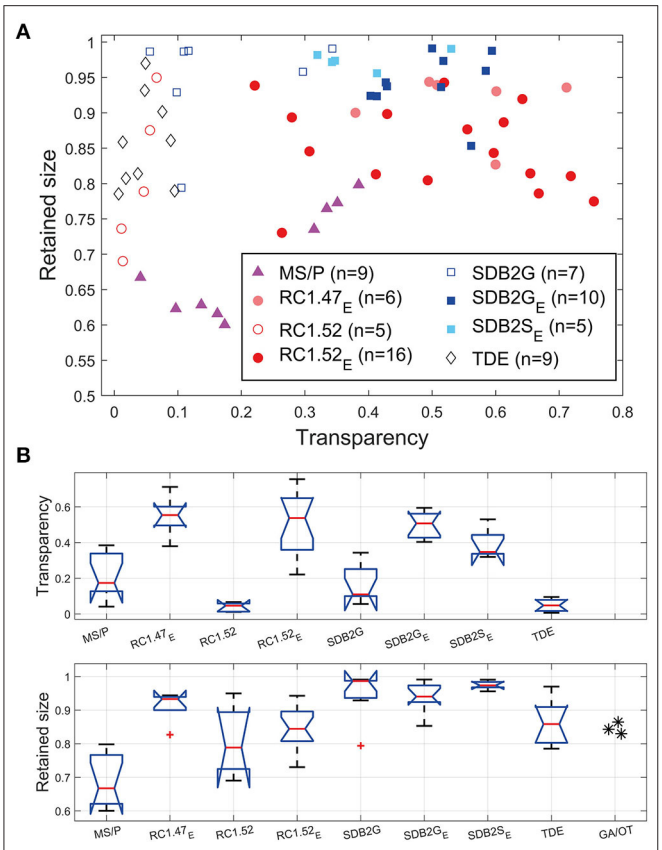

FIGURE 4 | Clearing performance measured using transparency and retained size. **(A)** A scatter plot of the transparency vs. retained brain size. "$_E$" stands for ethanol treatment. The parenthesis after the clearing method name (n = …) indicates the number of samples (brains). **(B)** Box plot (Matlab R2016b built-in boxplot function) showing median (red line), notches, 25th and 75th percentiles (edge of boxes), whiskers (extreme data points). MS/P always includes ethanol dehydration but no rehydration. Each transparency measurement was normalized using the medulla height to compensate for differences in brain thickness.

the medium. We might, therefore, expect not only differences in transparency between different variants of the same medium, but also in shrinkage due to potential water extraction from the tissue at high concentrations of the medium.

For our insect brains, both ethanol-treated variants of SeeDB2 gave good transparency, but the higher index variant, SeeDB2S$_E$, was actually worse than SeeDB2G$_E$ on average. The transparency performance for both Rapiclear1.52$_E$ and Rapiclear1.47$_E$ was among the best of the media tested and very similar to SeeDB2G$_E$, although once again if anything the lower refractive index variant actually gave slightly better transparency (**Figure 4B**). While these slight differences may be due to partial mismatch between the medium and the average refractive index of the fixed brain, we should note that SeeDB2S in particular is a very viscous medium, more so than either Rapiclear variant tested or the less concentrated iohexol solution (SeeDB2G): Despite our application of a dilution series to aid penetration before immersing brains in the final concentration, it may be that SeeDB2S is less likely to infiltrate key structures such as small tracheal tubes than the less viscous media.

Shrinkage was not a serious issue for any variant of the iohexol based media (SeeDB2), with the vast majority of brains retaining >90% of their original size (**Figure 4B**). Shrinkage of brains immersed in Rapiclear1.52$_E$ was around double that seen in the lower index version (Rapiclear1.47$_E$) which, like the SeeDB2 brains, retained almost 95% of their original size. While the exact composition of Rapiclear is currently proprietary, it includes glycerol with a maximum refractive of 1.473 at 100% concentration. Hence it is possible that the very high concentration of other reagents required to achieve a higher index (n = 1.52), leads to some water extraction from tissue and thus worse shrinkage compared to the lower refractive index variants. In terms of shrinkage, the widely applied MS/P technique was the worst protocol by far among those tested, with a median shrinkage to only 66.74% of the original size (**Figure 4B**). This gross change is immediately evident from the individual brain illustrated in **Figure 3E** before and after MS/P which we selected to illustrate our typical measurement landmarks.

It is likely that MS/P gives high shrinkage due to the ethanol dehydration (without rehydration) required before embedding, as well as through evaporation of the mounting medium solvent (toluene) following final mounting, which can also introduce unwanted bubbles and cavities into the space surrounding the brain. We wondered, however, whether this might also result in part from the limited crosslinking achieved by formaldehyde-only fixation. Most tissue fixation protocols for wholemount neuron imaging use relatively simple formaldehyde fixation in PBS, often using formaldehyde solutions made up from liquid stocks containing preservatives such as methanol to extend the shelf life, rather than freshly mixed paraformaldehyde (PFA) solution. While broadly compatible with many post-fixation treatments, such as immunohistochemistry, this may not provide optimal fixation and cross-linking of proteins and thus control over tissue shrinkage during subsequent dehydration. To provide an estimate of the minimum shrinkage possible if the same type of brain tissue is subjected to 'gold standard' optimal fixation, we therefore subjected a small number of brains to an electron microscopy (EM) preparation protocol. EM fixation combines both freshly mixed paraformaldehyde with the more strongly protein crosslinking fixative glutaraldehyde (GA), as well as post-fixation with osmium tetroxide (OT). The latter preserves lipid structures which would otherwise dissolved during alcohol dehydration following formaldehyde only fixation, potentially contributing to shrinkage during subsequent dehydration/embedding. Based on 3 GA/OT fixed and epoxy resin embedded brain samples we prepared, the average shrinkage was indeed substantially less than in MS/P mounted brains, with a mean retained size close 85% (see asterisks in **Figure 4B**, lower). It would require further work to establish whether this improvement following dehydration is due only to the fixatives used, or also to the non-solvent based embedding medium (since epoxy hardens though polymerization rather than solvent evaporation), or

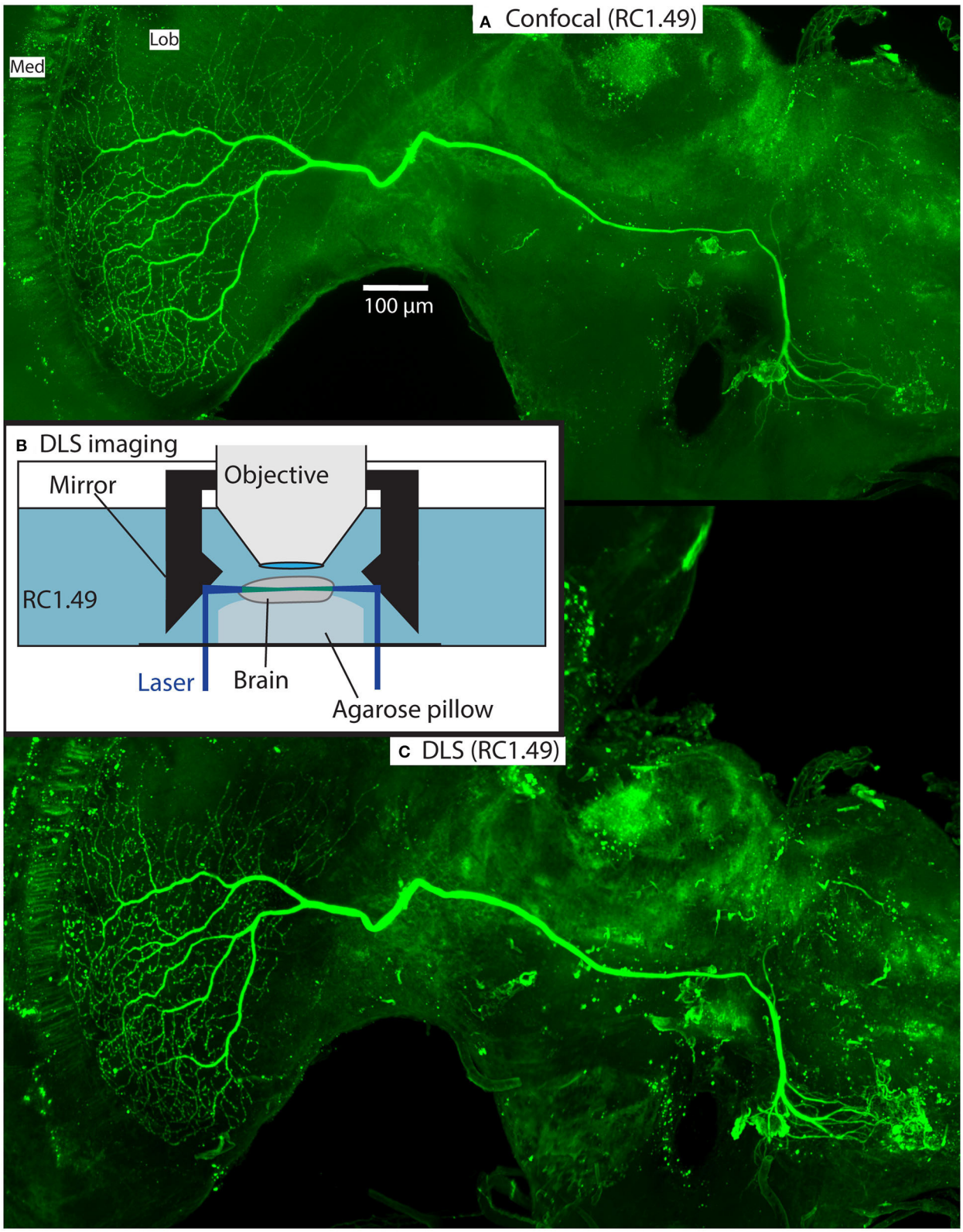

FIGURE 5 | Example of a Lucifer yellow injected wide-field motion neuron in a brain (#160) cleared with Rapiclear1.49$_E$. The neuron is a wide-field motion detector lobula complex neuron. The images were taken using a Leica SP8 DLS in confocal mode with a 20x oil immersion objective **(A)** and DLS mode with a 5x/0.15 objective and DLS TwinFlect 7.8 mm mirrors **(C)**. **(B)** illustrates the DLS imaging method used to acquire **(C)**.

both. Nevertheless, while this gave an improvement over MS/P embedding, the 'gold-standard' fixation treatment still clearly results in more shrinkage than we obtained with the best of water-miscible clearing media such as SeeDB2 or Rapiclear (**Figure 4B**).

Compatibility With Large Scale and Super-Resolution Imaging Techniques

Our analysis above shows that some of the more recently introduced clearing protocols with a lower refractive index (∼1.47), that better matches insect brain tissue, have great

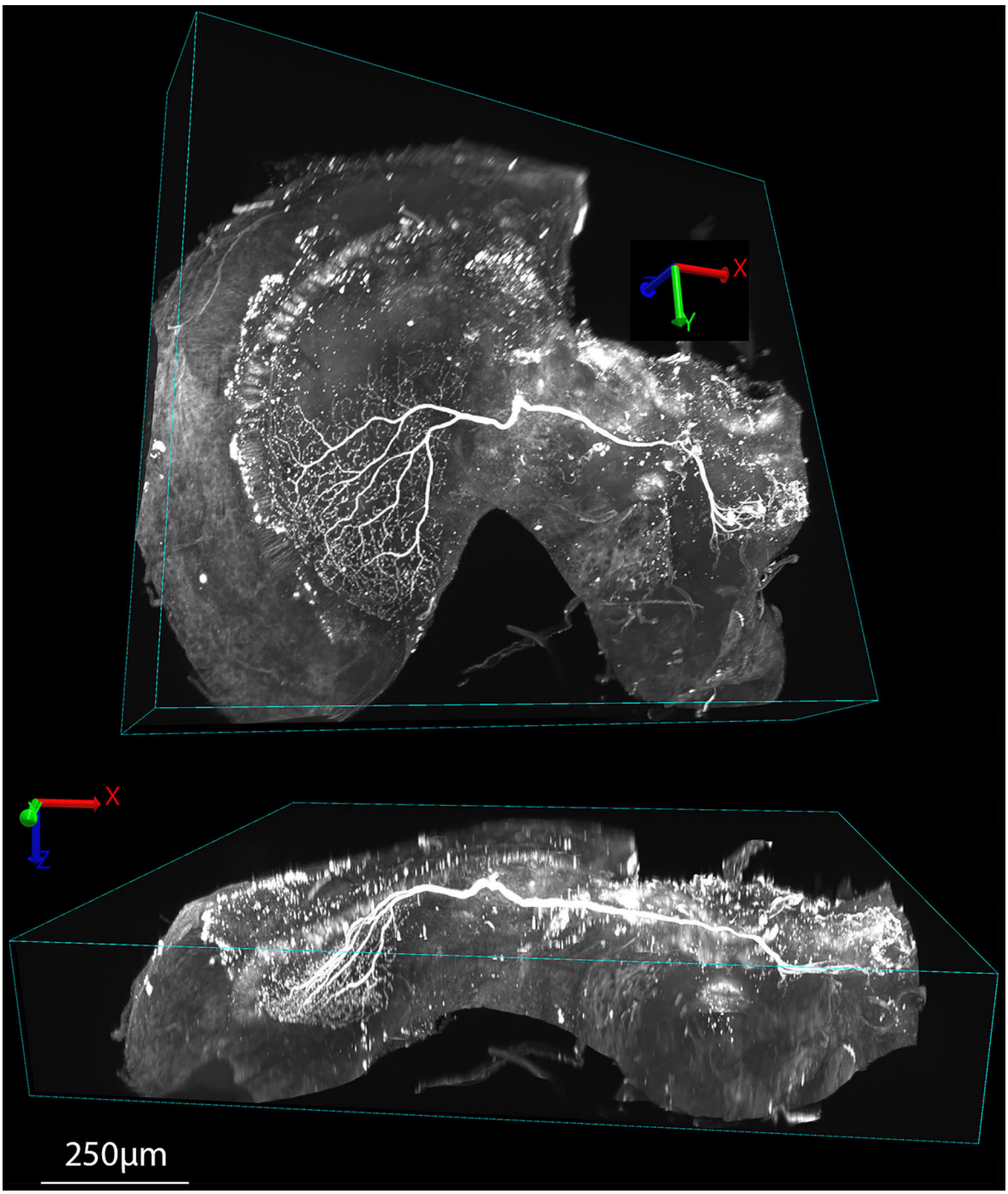

FIGURE 6 | Examples of 3D renderings of an XYZ series obtained in DLS imaging mode of a tracer injected wide-field motion neuron (the same sample as **Figure 5C**) cleared with Rapiclear1.49$_E$. The upper view shows the brain rotated roughly orthogonal to the main arborization of the neuron within the lobula complex, while the lower view is rotated to show this arborization side-on, illustrating the way the dendrites extend in a planar structure within the lobula plate, 250 µm below the sample surface.

potential for high quality whole-mount imaging. Rapiclear in particular involves a very simple sample preparation protocol (direct transfer to the medium from buffer following fixation and pre-treatment). In order to demonstrate the usefulness of this technique in real-world applications, we cleared a number of brains from the hoverfly *Eristalis* in Rapiclear following electrophysiological recording and intracellular injection of single neurons in the optic lobes with the fluorescent probe Lucifer yellow (see Additional Experiments and Example Treatments). We identified a number of large "tangential" neurons in these brains with neural processes ramifying throughout a range of depths within the outer lobula complex and then with projections of the axon 1 mm or more across the brain to contralateral midbrain structures. The large size of such neurons and the range of depths of their processes makes them challenging to image at high resolution in whole mount.

Figure 5 illustrates an example from one of the stained brains. This was a wide-field motion sensitive neuron with high sensitivity to downwards and rightward moving bars and grating patterns in the contralateral side of the visual field, suggesting that its inputs were the dendrites visible in the contralateral midbrain. The z-projection of the neuron in **Figure 5A** was obtained in the confocal microscope within a day of commencing the clearing process, illustrating the speed of the technique and the high quality of resulting images. In this case we used an intermediate refractive index (Rapiclear1.49) to provide a compromise between the slightly greater shrinkage of Rapiclear1.52 and the ideal medium for a 20x oil immersion objective, which gave us enough working distance to image through the full depth of the brain.

Figures 5C, **6**, **7** show the same sample as **Figure 5A** after 9 months of storage at room temperature (in darkness). For **Figure 5C** we exploited an additional advantage of the non-hardening medium by first removing one coverslip and simply rinsing off the old Rapiclear (which remained fluid) before re-mounting the sample so that it was suspended on an agarose pillow above the base of a glass-bottomed imaging well (**Figure 5B**) and then re-clearing overnight in fresh Rapiclear1.49. We then used the Leica SP8 DLS microscope in the 'Digital Light Sheet' (DLS) mode, which reflects a scanned light sheet into the brain from the sides using a pair of mirrors attached to the imaging objective, which in this case was immersed directly in the Rapiclear. Both the objective and mirror set were optimized for working in clearing media with the refractive index of Glycerol. For direct comparison with the confocal series in **Figure 5A,** we still imaged the brain in the same orientation as the confocal series, i.e., with the objective directed at the posterior brain surface and the Z axis corresponding to the anterior-posterior axis of the brain ("Posterior view"), which is the thinnest overall dimension of the insect brain. This imaging mode places high dependency on the degree of clearing, since excitation laser light has to pass through larger horizontal dimension of the sample e.g., through the ventral and dorsal margins of the medulla in order to excite fluorescence within the lobula. Any residual opacity in the medulla (or uncleared tracheae) casts shadow artifacts onto the resulting horizontally illuminated columns as the laser scans the light sheet. Despite the absolute resolution limits of the lower N.A. objective used for the DLS images, the overall quality of the image stacks was still excellent compared with the confocal images, especially considering the total imaging time required was only a few seconds (**Figures 5C**, **6** and **Supplementary Video 1**). To illustrate 3D imaging capability we generated **Supplementary Video 1** and example pictures in **Figure 6** showing the same wide-field motion neuron as in **Figure 5** but rendered in 3D.

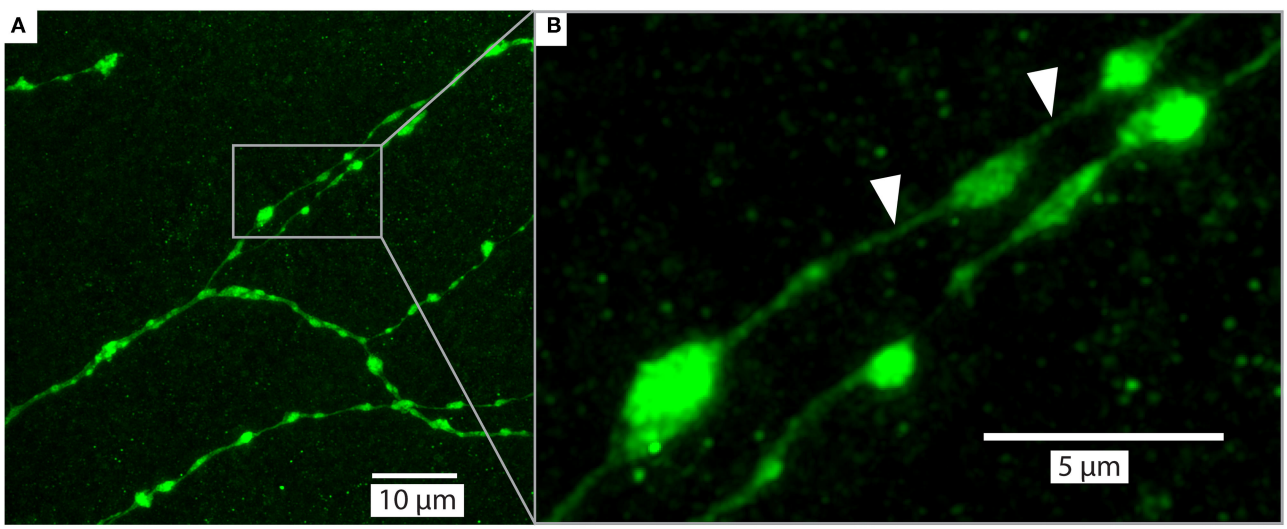

FIGURE 7 | Example of a detailed branches of a tracer injected wide-field motion neuron (same as **Figure 5**) in brain (#160) cleared with Rapiclear1.49$_E$ and imaged with a glycerol objective (63x, NA: 1.3). The images were captured from a sample following 9 months of storage in room temperature. The imaging depth was around 50µm bellow brain surface. **(A)** shows an overview of a group of branches and **(B)** zooms in on a subset to illustrate the details of a few "blebs," which are considered to be an indication that the branches have output synapses (Hausen, 1976; O'Carroll et al., 1992). The white arrows indicate very fine neurites that have a diameter of between 136 and 271 nm.

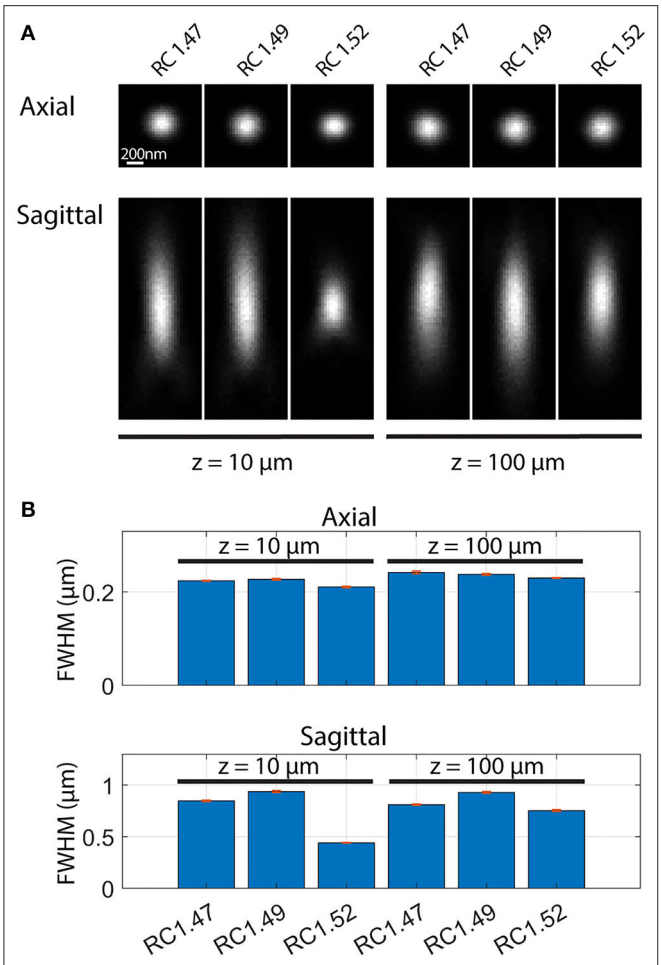

FIGURE 8 | Point spread functions **(A)** and full width at half maximum (FWHM) **(B)** of fluorescent nanobeads (diameter: 200 nm) embedded in agarose and Rapiclear1.47 (RC1.47, [63x, NA: 1.3]), Rapiclear1.49 (RC1.49, [63x, NA: 1.3]) and Rapiclear1.52 (RC1.52, [63x, NA: 1.4]) with different refractive indices and at different sample depth (z). **(B)** The bar plot shows average FWHM and SEM based on 5 samples. Each axial FWHM sample was an average of the vertical and horizontal FWHM. Sagittal FWHM was measured along the vertical axis.

Super-Resolution Imaging at Large Depths in Rapiclear

Upon the introduction of SeeDB2S and SeeDB2G, the authors who developed these media already highlighted their potential for application of a number of super-resolution imaging techniques. To explore the similar potential for Rapiclear, we obtained super-resolution images (**Figure 7**) from a detailed region of the lobula plate arborization of the same sample as in **Figure 5A**, again re-imaged 9 months after the initial clearing. These were obtained using the Leica SP8 microscope in "Hyvolution" mode, with a 0.5 Airy unit pinhole and 2x oversampling in X, Y, and Z, and a high numerical aperture 63x objective matched to glycerol immersion. Following acquisition, the image stack was first stabilized for 3-dimensional drift, before application of deconvolution using the high-resolution options in the Huygens software that provides the core to the Hyvolution mode. These images clearly resolve many very small diameter processes within the terminal dendrites (e.g., **Figure 7B** white arrows, neurite diameter 136–271 nm) lying between varicosities ("blebs") that are most likely clumps of mitochondria, as typically associated with output synapses in insect neurites (O'Carroll et al., 1992).

The excellent image resolution evident from **Figure 7** shows that the transparency and the optical match between the medium and objective must, in practice, be sufficient to achieve a high-quality point spread function (PSF), even at substantial depths within the sample. Since this has not been quantified previously for Rapiclear, we further estimated the effect of image depth on the PSF by imaging fluorescent nanobead samples prepared by suspending these in a sodium alginate hydrogel which was then cleared and mounted as for the insect brains (using either Rapiclear 1.47, 1.49, and 1.52). These were imaged either using a 63x objective for glycerol immersion (for Rapiclear 1.47, 1.49, objective NA = 1.3) or a 63x oil immersion objective (for Rapiclear 1.52, objective NA = 1.4) to try and optimize the match between clearing medium and objective immersion medium. At 100 µm depth, the PSF is elongated in the Z dimension (**Figure 8**), but otherwise comparable to a bead 10 µm below the coverslip. While minor, this elongation was somewhat surprising considering that the Rapiclear 1.52 medium should be an index match for oil immersion. It is possible that this is due to small amount of residual water retained within the cleared hydrogel suspension in which nanobeads were embedded to restrict their Brownian motion.

At shallow depths (10 µm) PSFs for the lower index Rapiclear variants are slightly more elongated in the Z dimension than in the oil immersion (1.52) condition, consistent with the higher numerical aperture of the latter objective. Importantly however, at 100 µm depth the PSFs for these media were similar to that obtained by oil immersion, particularly so for Rapiclear 1.47, which is closest to a perfect match for the glycerol immersion medium and which shows less obvious additional elongation along the Z axis compared with shallow depths (**Figure 8B**). Considering our earlier observation (**Figure 4B**) that the tissue clarity of both SeeDB2S and Rapiclear 1.52 were worse than their glycerol matched counterparts, it is likely that the effective refractive index of the brain tissue once fixed and cleared in these media is closer to 1.47 than to 1.52. Hence while the additional numerical aperture available for oil immersion may provide better resolution for very shallow samples, our results suggest that the best results for super-resolution imaging in very deep insect brain samples will come from applying a lower index clearing medium in combination with an objective matched to glycerol as the immersion medium, as we used in **Figure 7.**

DISCUSSION

Clearing Performance

In this paper, we limited our analysis to variations of four clearing methods shown previously to work well on insect brains. Our results and protocols provide objective grounds for other researchers to select between the tested clearing media for the one best suited to their specific application. Although it didn't perform optimally for our samples, TDE is relatively inexpensive. It is possible that we might have

seen improved clarity with further experimentation, either by additional pre-treatment with ethanol or with alternative dilutions to lower refractive index. Otherwise, despite their additional cost, the two recently introduced clearing media, SeeDB2G and Rapiclear, provide a superior degree of tissue clarity, shrinkage control and potential for high resolution imaging at large depths within insect brain samples, compared to traditional clearing media still used by many labs. The reduced tissue shrinkage in particular should be a serious consideration for any high-resolution application. Assuming that neuron structures shrink isometrically, the large shrinkage we quantified for the traditional methyl salicylate/Permount samples represents a very substantial loss of potential resolution during subsequent imaging, irrespective of the objective used. Although of course this is partially offset by having a smaller volume that requires imaging (and thus reduced objective working distance).

If long term storage or perfect mechanical stability during imaging are key considerations, there may still be compelling reasons to use permanent hardening mounting media such as Permount, for example. Although we have not yet had an opportunity to evaluate the very long-term storage potential of the Rapiclear technique, we have a number of samples stored simply in the dark exactly as initially prepared (i.e., mounted between two coverslips using a 500 μm self-adhesive plastic spacer) for well over a year at room temperature, and which still show excellent fluorescence. Indeed, the image in **Figure 7** was obtained from the identical sample to **Figure 5A** after 9 months of storage at room temperature. Nevertheless, MS/P is known to be safe for storing samples for years with preserved fluorescence and tissue quality.

Variability in Transparency and Shrinkage

Some clearing protocols, including MS/P and Rapiclear1.52$_E$ showed substantial variability in transparency between individuals (**Figure 4A**). This may in part reflect differences between species included in the analyses, even though we normalized this measure to account for variability in brain size. Potentially, certain species could be more easily cleared with some clearing methods, due to differences in tissue structure (including tracheal distribution). Such variation might also explain the poor performance of TDE in our study using Dipteran brains compared with the good clearing reported for this medium in an earlier study on dragonfly CNS tissue (Gonzalez-Bellido and Wardill, 2012). These differences may also result in part from variations in the dissection procedure (carried out in this case by more than one researcher), where some brains were left with more surface tracheal tubes and air sacks left on the brain, as can be seen in the uncleared brain in **Figure 2C**, for example (*cf* **Figures 2B,D**). This could affect transparency within the selected ROI since this was typically placed within the lobula, where such tracheae are prominent (see **Figure 1C**).

Role of Ethanol Pre-treatment

Ethanol pre-treatment greatly improved the clearing performance in all protocols in which it was used. Vacuum treatment on the other hand showed no obvious effect as we applied it, possibly due to limitations in the vacuum pressure we achieved. Why is ethanol treatment so effective? One possibility is that the low surface tension of ethanol, more than 3x lower than water (Vazquez et al., 1995) allows it to penetrate tissue and displace air better, particularly within the tiny tracheal tubes. Ethanol is widely used as an additive in many histological fixation procedures, to improve penetration of reagents such as aldehydes. Moreover, we note that the improved clearing may result from the fact that lipids are soluble in ethanol, and light scattering by lipid structures can impair visualization of cellular detail (Sun and Sun, 1985; Kacena et al., 2004; Troiano et al., 2009). Indeed, organic solvents can extract lipids or reduce refractive-index variations in a number of clearing methods, and electrophoretic removal of lipid micelles after solution by detergents in hydrogel stabilized tissues, followed by refractive index matching is the primary basis for the CLARITY clearing technique, and its derivations (Chung et al., 2013). Hence while both ethanol and vacuum treatment may contribute to removal of air from tracheal tubes, ethanol treatment may have broader, solvent related, effects on the tissue, leading to enhanced clearing performance, even though insect neurons lack myelination, so that the overall lipid content of the brain is lower than in mammalian tissue. While water extraction during ethanol dehydration leads to some shrinkage, we found that with adequate fixation, subsequent rehydration before clearing largely restored the tissue to its original volume.

Deep Tissue Imaging Techniques

In emerging deep-tissue imaging applications such as light-sheet imaging, a major advantage of aqueous miscible clearing media is their compatibility with a range of direct immersion objectives. The high degree of additional tissue transparency that we obtained with such media is another compelling reason to consider them for such applications. The tissue clarity was certainly adequate to get uniformly illuminated light sheet images of an adequate quality to allow for neuronal morphology 3D reconstruction for confirmation of neuronal identity or neuron subtype identification. Light-sheet microscopy ultimately falls short of the resolution available via other techniques, due in large part to the limited numerical aperture of the very long-working distance objectives typically employed. Nevertheless, the simplicity and speed of these clearing techniques offers some potential advantages for high-throughput analysis of neuronal structure compared with more traditional images obtained from multiple Z series by confocal imaging (which may take many hours per sample to acquire). Indeed, with the Leica SP8 DLS microscope system we used in this study, it is even possible to achieve near simultaneous imaging of the whole brain from above in the DLS mode, and confocal imaging from below (at least using air or water immersion objectives with a working distance long enough to reach the sample through the agarose pillow). Of course, confocal images are also directly available by simply remounting the sample between coverslips (which takes minutes) if even higher resolution imaging of key structures is required using shorter working distance objectives, e.g., for more detailed reconstructions for computational modeling studies where the interest lies in the fine neurites.

One downside to these newer media is that the reagents involved in both are relatively expensive, at least compared with methyl salicylate or TDE. They are either proprietary in the case of Rapiclear, or based on products made for human clinical use in the case of the Omnipaque used in SeeDB2. This may be a consideration for light sheet microscopy in particular, where the objective is immersed in the same medium, requiring a relatively large volume. In our own hands, we have found that this is mitigated by re-cycling some of the immersion medium for future imaging sessions, as well as by other advantages such as the ease of rinsing excess Rapiclear from the objectives afterwards in water. SeeDB2 is less suitable in this regard, as it tends to harden rapidly on contact with air.

Toxicity

The preparation of samples using the newer media, including TDE, SeeDB2 and Rapiclear is rapid and straightforward. TDE has low toxicity, and likewise, SeeDB2 is not considered to be seriously toxic (Schega et al., 2020), being widely injected intravenously as an X-ray contrast agent in humans/animals although can have adverse effects in large doses (Stuart et al., 2009). The chemical compounds of Rapiclear are not fully known due to pending patent (SunJin Lab Co.). The MSDS for this product notes only the presence of a small amount of preservative (Sodium azide) as a potential hazard. Since this is a commonly used additive in many of the immunohistochemical procedures frequently carried out in insect brain research prior to clearing anyway, it requires no special precautions beyond those generally already employed in most labs. The low toxicity of these compounds thus favor them over the traditional methyl salicylate and Permount method for insect tissue, with less risk of exposure to either the noxious smelling and toxic methyl salicylate or the toluene in Permount, which must be handled at all times in a fume cupboard. The fact that these clearing media have low toxicity and are safe to use on the open bench makes it easier to think in terms of robotic automation of experimental protocols which is becoming possible even for labs with lower sample output frequency (Savall et al., 2015; Gome et al., 2019; Poulsen et al., 2020).

Implications of a Less Viscous Mounting Medium

As noted earlier, SeeDB2G, Rapiclear, and TDE are less viscous compared to Permount, and particularly so once Permount is fully hardened by solvent evaporation. This has pros and cons. Obviously a less viscous medium may be better for penetrating thick volumes as well as generally easier to handle during the mounting process. However, during the very lengthy 2x-oversampling imaging required for super-resolution techniques, such as 3D deconvolution that we applied for **Figure 7**, we noted a slight drift in the sample position over time. While such minor drifts are common due to small temperature changes leading to stage expansion/contraction, it is possible that the less viscous mounting medium for our sample contributed to this, especially since our microscope uses an inverted objective pathway, requiring the sample to be positioned upside down compared to its storage position. Although our software (via the Huygens image stabilization plugin) was able to correct for this drift it could be worth considering storing such samples in their imaging position a few hours before imaging to minimize this type of drift. Alternatively, the thickness of the spacer used to suspend the brain between the two coverslips could be reduced so that the brain is gently compressed along the Z dimension. On the plus side, one benefit of using less viscous mounting medium as demonstrated here is that it is easy to remove the sample and remount it in another orientation if required (**Figure 5B**).

Alternative Clearing Methods and Future Work

Given the very high performance we observed for both Rapiclear and SeeDB2 in terms of low shrinkage, high clarity, low toxicity and relative simplicity, these should be seriously considered if insect tissue is the main target. Nevertheless, the protocols we assessed here represent only a subset of a diverse range of alternative clearing methods and combinations with pre-treatment methods now available, many of which may be more optimal for other tissue types or lower resolution applications, particularly in whole brain imaging of mammals. Because of the much smaller size of the insect brain, the optimal clearing media for insect brains need to be compatible with higher index immersion media, bringing with it similar demands and compromises to those for high-resolution microscopy in cleared mammalian brain tissue. In introducing SeeDB2 as a good alternative for such super-resolution applications, Ke et al. (2016) compared the point-spread function (PSF) in images of fluorescent nanobeads for a number of additional clearing media that have been widely employed across a range of species, particularly rodents. Their results confirmed well-controlled expansion of the PSF at depths of 100 μm for tunable media such as TDE and SeeDB2, due most likely to a reduction in spherical aberration. Although Rapiclear was not included in the Ke et al. (2016) analysis, we also see this property for this medium when correctly index-matched to the objective. By contrast, a number of other widely employed media included in their analysis gave clearly inferior PSFs by a depth of 100 μm and correspondingly more rapid fall off in brightness with imaging depth. These included Scale/S, ProLongGold, FocusClear, and CUBIC, many of which have lower refractive index than is optimal for avoiding spherical aberration at depth when using higher numerical aperture objectives.

The low index of a medium such as FocusClear is necessary to achieve good clarity in tissue after application of specialized hydrogel lipid-substitution methods for clearing large mammalian organs, which form the basis of the CLARITY method (Chung et al., 2013; Tomer et al., 2014) and a number of derivative protocols. While FocusClear is proprietary, less expensive alternatives such as dilute TDE or glycerol can be substituted with varying degrees of success (Tomer et al., 2014; Costantini et al., 2015). Several microscope manufacturers have now developed direct immersion objectives compatible with lower index clearing media such as Sca*l*eS or FocusClear, providing working distances up to several mm (Hama et al., 2015; Liu et al., 2016). However, the very large size of such objectives

and the specific match to a single immersion medium requires an upright microscope system dedicated to the goal of imaging this specific tissue type. Despite a direct immersion optical designs that do not need to deal with the additional thickness of the coverslip, the numerical aperture available for such objectives is still limited by the lower index of the medium, typically to around 1.0. Hence while such dedicated imaging pipelines and systems are providing unprecedented insights at remarkable resolution, deep into structures imaged within cleared brains in zebrafish, mouse or even humans (Chung et al., 2013; Hama et al., 2015), they are less suitable for very high resolution applications. Furthermore, loss of antigenicity is a problem with these techniques, particularly for transmembrane proteins, with up to 65% of the protein lost during lipid substitution (Chung et al., 2013), a problem that can only be partially remedied by secondary reagent amplification (Li et al., 2017). Finally, methods such as CLARITY involve extended protocols, special equipment and application of highly toxic compounds such as acrylamide.

Several more recently developed techniques have attempted to overcome these limitations. Like the compounds we evaluated here, these methods also exploit tunable refractive index media. These new methods may also be suitable for high resolution applications, although to the best of our knowledge they have yet to be tested in insect brains. Examples include OPTIClear (Lai et al., 2018) and Ce3D (Li et al., 2017). The tunability of refractive index in the first two of these methods results from the inclusion of essentially similar ingredients to those in the tunable media we used in the present study. OPTIClear is specifically optimized for human brain tissue, and is primarily based on a mixture of the TDE and iohexol. The addition of an additional compound, N-methylglucamine may have some benefit for human brain tissue, hence may also be useful for insects given sufficient effort in developing additional protocols. Like SeeDB2, Ce3D is also an iohexol-based medium, with the addition a of a small percentage of *N*-methylacetamide (Li et al., 2017). A recently reported novel medium, MACS (Zhu et al., 2020) is based on m-xylylenediamine, an interesting material, with a refractive index tunable up to 1.57. This appears to offer promise of good tissue clarity without lipid extraction and short processing times, although at the expense of m-xylylenediamine being highly toxic, which we note is a specific advantage of SeeDB2 and Rapiclear.

DATA AVAILABILITY STATEMENT

The raw data supporting the conclusions of this article will be made available by the authors, without undue reservation.

AUTHOR CONTRIBUTIONS

DO'C, BB, and HF: conceptualization. BB and HF: clearing experiments and measurements. BB: tracer injection. BB and DO'C: confocal imaging and manuscript writing. DO'C: DLS imaging. ER, DO'C, and BB: bead experiments. All authors: comments on figures and writing.

FUNDING

The research was funded by the Swedish research council (Vetenskapsrådet, VR 621-2014-4904, VR 2018-03452) and Formas (project grant # 2018-01218).

ACKNOWLEDGMENTS

We thank Seán McGovern for his help with brain dissections and data registration. We acknowledge the Microscopy Facility at the Department of Biology, Lund University, and in particular Ola Gustafsson for assistance with confocal microscopy and electron microscopy sample preparation, and Thommie Karlsson from Micromedic AB for assistance with light sheet microscopy.

SUPPLEMENTARY MATERIAL

The Supplementary Material for this article can be found online at: https://www.frontiersin.org/articles/10.3389/fnana.2020.599282/full#supplementary-material

Supplementary File 1 | Transparency and size measurements and meta-data.

Supplementary Video 1 | Video of a light sheet imaged neuron and brain rendered in 3D.

REFERENCES

Adden, A., Wibrand, S., Pfeiffer, K., Warrant, E., and Heinze, S. (2020). The brain of a nocturnal migratory insect, the Australian Bogong moth. *J. Comp. Neurol.* 528, 1942–1963. doi: 10.1002/cne.24866

Ariel, P. (2017). A beginner's guide to tissue clearing. *Int. J. Biochem. Cell Biol.* 84, 35–39. doi: 10.1016/j.biocel.2016.12.009

Barnett, P. D., Nordström, K., and O'Carroll, D. C. (2007). Retinotopic organization of small-field-target-detecting neurons in the insect visual system. *Curr. Biol.* 17, 569–578. doi: 10.1016/j.cub.2007.02.039

Bekkouche, B., Shoemaker, P. A., Fabian, J., Rigosi, E., Wiederman, S. D., and O'Carroll, D. C. (2017). "Multicompartment simulations of NMDA receptor based facilitation in an insect target tracking neuron," in *Artificial Neural Networks and Machine Learning – ICANN 2017. Lecture Notes in Computer Science*, eds A. Lintas, S. Rovetta, P. Verschure, and A. Villa (Cham: Springer), 397–404.

Carrow, G. M., Calabrese, R. L., and Williams, C. M. (1984). Architecture and physiology of insect cerebral neurosecretory cells. *J. Neurosci.* 4, 1034–1044. doi: 10.1523/JNEUROSCI.04-04-01034.1984

Chung, K., Wallace, J., Kim, S. Y., Kalyanasundaram, S., Andalman, A. S., Davidson, T. J., et al. (2013). Structural and molecular interrogation of intact biological systems. *Nature* 497, 332–337. doi: 10.1038/nature12107

Coss, R. G., Brandon, J. G., and Globus, A. (1980). Changes in morphology of dendritic spines on honeybee calycal interneurons associated with cumulative nursing and foraging experiences. *Brain Res.* 192, 49–59. doi: 10.1016/0006-8993(80)91007-0

Costantini, I., Ghobril, J. P., Di Giovanna, A. P., Allegra Mascaro, A. L., Silvestri, L., Müllenbroich, M. C., et al. (2015). A versatile clearing agent for multi-modal brain imaging. *Sci. Rep.* 5:9808. doi: 10.1038/srep09808

Dong, C. Y., Yu, B., Kaplan, P. D., and So, P. T. C. (2004). Performances of high numerical aperture water and oil immersion objective in deep-tissue, multi-photon microscopic imaging of excised human skin. *Microsc. Res. Tech.* 63, 81–86. doi: 10.1002/jemt.10431

Dunbier, J. R., Wiederman, S. D., Shoemaker, P. A., and O'Carroll, D. C. (2012). Facilitation of dragonfly target-detecting neurons by slow moving features on continuous paths. *Front. Neural Circuits* 6:79. doi: 10.3389/fncir.2012.00079

el Jundi, B., Heinze, S., Lenschow, C., Kurylas, A., Rohlfing, T., and Homberg, U. (2010). The locust standard brain: a 3D standard of the central complex as a platform for neural network analysis. *Front. Syst. Neurosci.* 3:9. doi: 10.3389/neuro.06.021.2009

Frank, D. D., Enjin, A., Jouandet, G. C., Zaharieva, E. E., Para, A., Stensmyr, M. C., et al. (2017). Early integration of temperature and humidity stimuli in the Drosophila brain. *Curr. Biol.* 27, 2381–2388.e4. doi: 10.1016/j.cub.2017.06.077

Geurten, B. R. H., Nordström, K., Sprayberry, J. D. H., Bolzon, D. M., and O'Carroll, D. C. (2007). Neural mechanisms underlying target detection in a dragonfly centrifugal neuron. *J. Exp. Biol.* 210, 3277–3284. doi: 10.1242/jeb.008425

Gome, G., Waksberg, J., Grishko, A., Wald, I. Y., and Zuckerman, O. (2019). "OpenLH: open Liquid-Handling System for Creative Experimentation with Biology," in *Proceedings of the Thirteenth International Conference on Tangible, Embedded, and Embodied Interaction* TEI '19 (New York, NY: Association for Computing Machinery), 55–64.

Gonzalez-Bellido, P. T., and Wardill, T. J. (2012). Labeling and confocal imaging of neurons in thick invertebrate tissue samples. *Cold Spring Harb. Protoc.* 7, 969–983. doi: 10.1101/pdb.prot069625

Hama, H., Hioki, H., Namiki, K., Hoshida, T., Kurokawa, H., Ishidate, F., et al. (2015). ScaleS: an optical clearing palette for biological imaging. *Nat. Neurosci.* 18, 1518–1529. doi: 10.1038/nn.4107

Harvard, D., Richardson, S., and Lichtman, J. W. (2015). Clarifying tissue clearing. *Cell* 162, 246–257. doi: 10.1016/j.cell.2015.06.067

Hausen, K. (1976). Functional characterization and anatomical identification of motion sensitive neurons in the lobula plate of the blowfly calliphora erythrocephala. *Zeitschrift fur Naturforsch. Sect. C J. Biosci.* 31, 629–634. doi: 10.1515/znc-1976-9-1001

Heinze, S., Florman, J., Asokaraj, S., El Jundi, B., and Reppert, S. M. (2013). Anatomical basis of sun compass navigation II: the neuronal composition of the central complex of the monarch butterfly. *J. Comp. Neurol.* 521, 267–298. doi: 10.1002/cne.23214

Heinze, S., and Homberg, U. (2008). Neuroarchitecture of the central complex of the desert locust: intrinsic and columnar neurons. *J. Comp. Neurol.* 511, 454–478. doi: 10.1002/cne.21842

Kacena, M. A., Troiano, N. W., Coady, C. E., and Horowitz, M. C. (2004). Effects of ethanol post-fixation on the histological, histochemical, and immunohistochemical analysis of murine bone specimens. *J. Histotechnol.* 27, 15–20. doi: 10.1179/his.2004.27.1.15

Ke, M. T., Nakai, Y., Fujimoto, S., Takayama, R., Yoshida, S., Kitajima, T. S., et al. (2016). Super-resolution mapping of neuronal circuitry with an index-optimized clearing agent. *Cell Rep.* 14, 2718–2732. doi: 10.1016/j.celrep.2016.02.057

Keles, M. F., and Frye, M. A. (2017). Object-detecting neurons in *Drosophila*. *Curr. Biol.* 27, 680–687. doi: 10.1016/j.cub.2017.01.012

Kurylas, A. E., Rohlfing, T., Krofczik, S., Jenett, A., and Homberg, U. (2008). Standardized atlas of the brain of the desert locust, *Schistocerca gregaria*. *Cell Tissue Res.* 333, 125–145. doi: 10.1007/s00441-008-0620-x

Lai, H. M., Liu, A. K. L., Ng, H. H. M., Goldfinger, M. H., Chau, T. W., Defelice, J., et al. (2018). Next generation histology methods for three-dimensional imaging of fresh and archival human brain tissues. *Nat. Commun.* 9:1066. doi: 10.1038/s41467-018-05089-5

Li, W., Germain, R. N., and Gerner, M. Y. (2017). Multiplex, quantitative cellular analysis in large tissue volumes with clearing-enhanced 3D microscopy (Ce3D). *Proc. Natl. Acad. Sci. U.S.A.* 114, E7321–E7330. doi: 10.1073/pnas.1708981114

Lin, C., and Strausfeld, N. J. (2012). Visual inputs to the mushroom body calyces of the whirligig beetle dineutus sublineatus: modality switching in an insect. *J. Comp. Neurol.* 520, 2562–2574. doi: 10.1002/cne.23092

Liu, A. K. L., Hurry, M. E. D., Ng, O. T. W., DeFelice, J., Lai, H. M., Pearce, R. K. B., et al. (2016). Bringing CLARITY to the human brain: visualization of Lewy pathology in three dimensions. *Neuropathol. Appl. Neurobiol.* 42, 573–587. doi: 10.1111/nan.12293

Loren, M., Crouzet, C., Bahani, A., Vasilevko, V., and Choi, B. (2019). Optical clearing potential of immersion-based agents applied to thick mouse brain sections. *PLoS ONE* 14:e0216064. doi: 10.1371/journal.pone.0216064

O'Carroll, D. C., Osorio, D., James, A. C., and Bush, T. (1992). Local feedback mediated via amacrine cells in the insect optic lobe. *J. Comp. Physiol. A* 171, 447–455. doi: 10.1007/BF00194577

Poulsen, K. M., Pho, T., Champion, J. A., and Payne, C. K. (2020). Automation and low-cost proteomics for characterization of the protein corona: experimental methods for big data. *Anal. Bioanal. Chem.* 6543–6551. doi: 10.1007/s00216-020-02726-1

Savall, J., Ho, E. T. W., Huang, C., Maxey, J. R., and Schnitzer, M. J. (2015). Dexterous robotic manipulation of alert adult *Drosophila* for high-content experimentation. *Nat. Methods* 12, 657–660. doi: 10.1038/nmeth.3410

Schega, Y., Flinner, N., and Hansmann, M.-L. (2020). Quantitative assessment of optical clearing methods on formalin-fixed human lymphoid tissue. *Pathol. Res. Pract.* 216:153136. doi: 10.1016/j.prp.2020.153136

Schmitt, J. M., and Kumar, G. (1998). Optical scattering properties of soft tissue: a discrete particle model. *Appl. Opt.* 37:2788. doi: 10.1364/AO.37.002788

Shoemaker, P. (2011). "Multicompartment simulations of NMDA receptor-based facilitation in insect visual neurons," in *Proceedings of 2011 7th International Conference on Intelligent Sensors, Sensor Networks and Information Processing (ISSNIP)* (Adelaide, SA), 85–90.

Silvestri, L., Costantini, I., Sacconi, L., and Pavone, F. S. (2016). Clearing of fixed tissue: a review from a microscopist's perspective. *J. Biomed. Opt.* 21:081205. doi: 10.1117/1.JBO.21.8.081205

Staudt, T., Lang, M. C., Medda, R., Engelhardt, J., and Hell, S. W. (2007). 2,2'-Thiodiethanol: a new water soluble mounting medium for high resolution optical microscopy. *Microsc. Res. Tech.* 70, 1–9. doi: 10.1002/jemt.20396

Stöckl, A. L., and Heinze, S. (2015). A clearer view of the insect brain—combining bleaching with standard whole-mount immunocytochemistry allows confocal imaging of pigment-covered brain areas for 3D reconstruction. *Front. Neuroanat.* 9:121. doi: 10.3389/fnana.2015.00121

Stuart, M. C., Kouimtzi, M., and Hill, S. R. (2009). *WHO Model Formulary 2008*. World Health Organization.

Sun, G. Y., and Sun, A. Y. (1985). Ethanol and membrane lipids. *Alcohol. Clin. Exp. Res.* 9, 164–180. doi: 10.1111/j.1530-0277.1985.tb05543.x

Tomer, R., Ye, L., Hsueh, B., and Deisseroth, K. (2014). Advanced CLARITY for rapid and high-resolution imaging of intact tissues. *Nat. Protoc.* 9, 1682–1697. doi: 10.1038/nprot.2014.123

Troiano, N. W., Ciovacco, W. A., and Kacena, M. A. (2009). The effects of fixation and dehydration on the histological quality of undecalcified murine bone specimens embedded in methylmethacrylate. *J. Histotechnol.* 32, 27–31. doi: 10.1179/his.2009.32.1.27

Tuchin, V. V. (2005). Optical clearing of tissues and blood using the immersion method. *J. Phys. D. Appl. Phys.* 38, 2497–2518. doi: 10.1088/0022-3727/38/15/001

Tuchin, V. V., Zimnyakov, D. A., Maksimova, I. L., Akchurin, G. G., Mishin, A. A., Utz, S. R., et al. (1998). Coherent, low-coherent, and polarized light interaction with tissues undergoing refractive-index matching control. *Coherence Domain Opt. Methods Biomed. Sci. Clin. Appl. II* 3251, 12–21. doi: 10.1117/12.306040

Vazquez, G., Alvarez, E., and Navaza, J. M. (1995). Surface tension of alcohol + water from 20 to 50°C. *J. Chem. Eng. Data* 40, 611–614. doi: 10.1021/je00019a016

Wan, P., Zhu, J., Xu, J., Li, Y., Yu, T., and Zhu, D. (2018). Evaluation of seven optical clearing methods in mouse brain. *Neurophotonics* 5:1. doi: 10.1117/1.NPh.5.3.035007

Xu, J., Ma, Y., Yu, T., and Zhu, D. (2019). Quantitative assessment of optical clearing methods in various intact mouse organs. *J. Biophotonics* 12, 15–20. doi: 10.1002/jbio.201800134

Yu, T., Qi, Y., Gong, H., Luo, Q., and Zhu, D. (2018). Optical clearing for multiscale biological tissues. *J. Biophotonics* 11:e201700187. doi: 10.1002/jbio.201700187

Zhu, J., Yu, T., Li, Y., Xu, J., Qi, Y., Yao, Y., et al. (2020). MACS: rapid aqueous clearing system for 3D mapping of intact organs. *Adv. Sci.* 7:1903185. doi: 10.1002/advs.201903185

Conflict of Interest: The authors declare that the research was conducted in the absence of any commercial or financial relationships that could be construed as a potential conflict of interest.